

# Modelling the equilibrium height of offshore sand waves

---

MASTER THESIS



---

WIETSE VAN GERWEN BSc  
Enschede, September 23, 2016

# Modelling the equilibrium height of offshore sand waves

---

MASTER THESIS

WATER ENGINEERING & MANAGEMENT  
FACULTY OF ENGINEERING TECHNOLOGY  
UNIVERSITY OF TWENTE

<b>Author</b>	Wietse van Gerwen BSc
<b>Contact</b>	wietsevangerwen@gmail.com
<b>Thesis defence date</b>	September 30, 2016
<b>Graduation committee</b>	
<b>Graduation supervisor</b>	Prof. Dr. S.J.M.H. Hulscher
<b>Daily supervisors</b>	Dr. ir. B.W. Borsje Ir. J.H. Damveld

Enschede, September 23, 2016

---

**UNIVERSITY OF TWENTE.**

# Preface

Before you lays the result of my master thesis, conducted at the Water Engineering and Management department of the University of Twente. The outcomes of the study are presented in paper format, which I intend to submit later this year. Because not all aspects of my studies were necessary to convey the message of the paper, some appendices are added. Looking back on the long process that led to this writing, I must say, I really enjoyed doing this.

Of course, I would not have been able to come to this point without the help of my supervisors and support of my friends and family. Therefore, I would like to thank Suzanne for the helpful writing tips and trust towards the end of the process. Johan, we had fruitful discussions at points I really needed some guidance, thank you for that. Last but foremost, I would like to thank Bas for giving me the opportunity to start on this subject. Throughout the whole process you have been able to motivate me with your enthusiasm and interest. I always felt welcome and I very much appreciate that you took the time for our many discussions and mail conversations.

*Wietse van Gerwen,  
Enschede, September 23, 2016*

# Contents

<b>1</b>	<b>Modelling the effect of suspended load transport and tidal asymmetry on the growth of tidal sand waves</b>	<b>2</b>
1.1	Abstract . . . . .	2
1.2	Introduction . . . . .	3
1.3	Model description . . . . .	5
1.4	Results . . . . .	9
1.5	Discussion . . . . .	15
1.6	Conclusions . . . . .	16
<b>A</b>	<b>Sensitivity of results to various parameters</b>	<b>22</b>
<b>B</b>	<b>Data analysis of field measurements after a dredging event</b>	<b>25</b>
B.1	Method . . . . .	25
B.2	Results . . . . .	26
B.3	Conclusion . . . . .	28

# Chapter 1

## Modelling the effect of suspended load transport and tidal asymmetry on the growth of tidal sand waves

W. van Gerwen, B.W. Borsje, J.H. Damveld, S.J.M.H. Hulscher

### 1.1 Abstract

Tidal sand waves are dynamic bed forms found in shallow seas, reaching heights of several meters and migration rates of several meters per year. Because of their dynamic behavior, unraveling the physical processes behind the growth of these bed forms is of particular interest to offshore industries. Various modelling efforts looking into the linear formation processes of sand waves already give a good description of the initial stages of formation. However, the non-linear evolution, causing sand waves to grow towards an equilibrium, is not yet fully understood. To further increase our understanding of the processes controlling the non-linear evolution of sand wave fields, a numerical shallow water model (Delft3D) is used. This is the first model study which shows the growth of a sand wave field towards a stable equilibrium.

It is shown that both suspended load transport and tidal asymmetry reduce the equilibrium sand wave height. A residual current results in the formation of asymmetrical bed forms that migrate in the direction of the residual current. By including suspended load transport and tidal asymmetry, the predicted equilibrium wave heights approximate wave heights as found in the field.

## 1.2 Introduction

Shallow seas have regular bed forms of various shapes and sizes. The largest of these bed forms are tidal sand waves and tidal sand banks. The wave lengths of these rhythmic features are in the order of hundreds of meters to several kilometres, respectively. Sand waves and sand banks are primarily located in sandy shelf seas with strong tidal currents. The evolution of the bed is described by the morphological loop, which is the interplay of hydrodynamics, sediment transport and morphology (Roos and Hulscher, 2003). Sand banks are up to tens of metres in height (Dyer and Huntley, 1999). They are less dynamic than sand waves; the migration rate of sand banks is an order of magnitude smaller than the migration rate of sand waves (Knaapen, 2005). This makes them of less interest to offshore operations. Typical migration rates for sand waves are in the order of 1 to 10 m/year (e.g. Besio et al., 2004; Knaapen, 2005), but can go up to tens of metres in areas with strong tidal currents (Terwindt, 1971). The height of sand waves is in the order of metres (typically 1 to 10 m) (e.g. McCave, 1971; Besio et al., 2004). An example of a sand wave field is shown in fig. 1.1, where a sand wave field off the coast of IJmuiden, the Netherlands, is visualised.

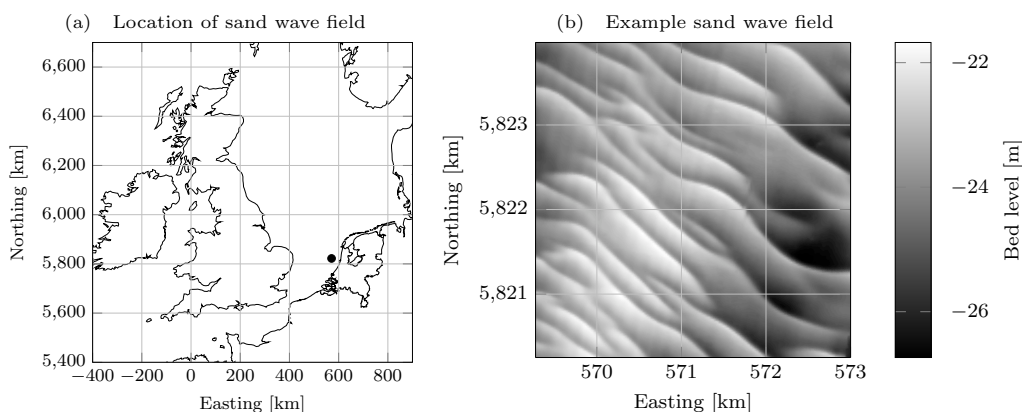


Figure 1.1 Example of a sand wave field (b), with its geographical location in the North Sea (a). Data courtesy of Ir. J.M. Damen.

The dynamic behaviour and dimensions of sand waves makes understanding their evolution of particular importance to offshore activities. For instance, sand waves can affect the navigation depth and stability of offshore platforms, pipelines and wind turbines, as shown by Németh et al. (2003). Knowledge about seabed dynamics could improve the design and increase the interval between surveys, so costs are reduced (Besio et al., 2008). Therefore, coastal managers are in need for tools to formulate design criteria. This makes insight in the processes controlling sand wave dynamics essential.

Hulscher (1996) explained the formation of sand waves as follows. Sand waves are generated by small perturbations of the seabed that cause flow alterations. The

flow is accelerated on the stoss side of the perturbation due to decreasing water depths, leaving smaller flows at the lee side due to increasing water depths. Because of the oscillating behaviour of the tide this happens in both directions, causing residual circulation cells when looking at tide-averaged flow values. This results in a net transport of sediment towards the crest. The opposing factor, gravity, causes transport from crest to trough. It is the balance between these two forces that determines the preferred wave length.

Various modelling studies have tried to increase our understanding of sand wave characteristics, where a clear distinction can be made between linear and non-linear models. Linear stability models are used to predict the initial stages of formation of small-amplitude sand waves. The model introduced by *Hulscher* (1996), was later extended by *Gerkema* (2000); *Komarova and Hulscher* (2000); *Besio et al.* (2003). Tidal asymmetry was investigated by *Németh et al.* (2002); *Besio et al.* (2004) and a depth dependent eddy viscosity with a no-slip condition at the bed was introduced by *Blondeaux and Vittori* (2005a,b); *Besio et al.* (2006). *Van Oyen and Blondeaux* (2009) looked into grain sorting and *Borsje et al.* (2009) investigated the effect of biota on the sand wave length. These models predict the fastest growing sand wave length, i.e. the fastest growing mode ( $L_{FGM}$ ). This mode is assumed to prevail due to the weakly non-linearity of the system (*Dodd et al.*, 2003). So far these modelling practices have been able to predict the sand wave characteristics (wave length, migration rate, crest orientation) during the initial stages of formation fairly well.

To reach an equilibrium, sand wave growth needs to reduce in time, for which non-linear terms need to be introduced. This is done in non-linear stability models, which build on the linear models (e.g. *Németh et al.*, 2006, 2007; *Sterlini et al.*, 2009). Calculations in these models are done on a domain with the length equal to the  $L_{FGM}$ , because the growth of very long sand waves is unsuppressed (*Van den Berg et al.*, 2012). With this restriction, these type of models can predict growth towards a stable equilibrium. However, the calculated wave heights are unrealistically large. *Van den Berg et al.* (2012) were the first to use such a model to investigate the growth of sand waves in a sand wave field, but no stable equilibrium was reached for the presented time period.

Another tree of models are the numerical shallow water models. One such model is Delft3D in which the complex interaction of many processes are solved by means of a numerical scheme (*Lesser et al.*, 2004). *Borsje et al.* (2013, 2014) used this model to successfully predict the initial stages of formation. This model enables the investigation of sand waves growth towards equilibrium. For this a sand wave field can be used, without the restriction of a domain with the length of the  $L_{FGM}$ , because the growth of very long sand waves is suppressed. This is caused the combination of an advanced turbulence model and suspended load transport (*Borsje et al.*, 2014).

In this paper we are interested in modelling the growth of sand waves towards a stable equilibrium. In particular, we would like to identify the processes that cause the overestimation of the equilibrium height in non-linear stability sand wave models

(e.g. *Van den Berg et al.*, 2012). The inclusion of suspended sediment transport in the model equations has already shown promising effects during the initial growth by suppressing long sand waves. For the long term this could prove a good addition. Also, the inclusion of a residual current resulted in better wave height predictions (*Sterlini et al.*, 2009).

The aim of this paper is to uncover the physical processes influencing the growth and equilibrium height of sand wave fields. This is done by using the numerical shallow water model (Delft3D) as presented in *Borsje et al.* (2014) and running it for long periods of time.

Chapter 1 describes the model set-up. The modelled influence of suspended load sediment transport and the residual current strength on the equilibrium conditions are then presented in section 1.4. The model set-up and results are discussed in section 1.5, followed by the conclusions in section 1.6.

### 1.3 Model description

The formation of sand waves is modelled using the numerical process-based model Delft3D (*Lesser et al.*, 2004). Using this model, *Borsje et al.* (2013) modelled the initial stages of sand wave formation, which they later extended by including suspended load transport in *Borsje et al.* (2014). Here, we limit to a summarized model description and refer the interested reader to *Borsje et al.* (2013, 2014) for a detailed model description.

#### 1.3.1 Hydrodynamics

The system of equations consists of the Navier-Stokes equations, flow- and sediment continuity equations and sediment transport equations. The vertical momentum equation is reduced to the hydrostatic pressure relation as vertical accelerations are assumed to be small compared to gravitational acceleration. The model equations are solved by applying  $\sigma$ -layering in the vertical. In this study, the model is run in the two-dimensional vertical (2DV) mode, i.e. considering flow and variation in  $x$  and  $z$  direction only, while assuming zero flow and uniformity in  $y$  direction and ignoring Coriolis effects. At the length scales of sand waves, Coriolis effects have been shown to have a negligible effect (*Hulscher*, 1996).

In terms of the  $\sigma$  coordinates, the 2DV hydrostatic shallow water equations are described by

$$\frac{\partial u}{\partial t} + u \frac{\partial u}{\partial x} + \frac{\omega}{(H + \zeta)} \frac{\partial u}{\partial \sigma} = -\frac{1}{\rho_w} P_u + F_u + \frac{1}{(H + \zeta)^2} \frac{\partial}{\partial \sigma} \left( \nu_T \frac{\partial u}{\partial \sigma} \right), \quad (1.1)$$

$$\frac{\partial \omega}{\partial \sigma} = -\frac{\partial \zeta}{\partial t} - \frac{\partial [(H + \zeta)u]}{\partial x}. \quad (1.2)$$

Here  $u$  is the horizontal velocity,  $\omega$  the vertical velocity relative to the moving vertical  $\sigma$  plane,  $\rho_w$  the water density,  $H$  the water depth below reference datum,  $\zeta$  the

free surface elevation,  $P_u$  the hydrostatic pressure gradient and  $F_u$  describes the horizontal exchange of momentum due to turbulent fluctuations. The vertical eddy viscosity  $\nu_T$  is calculated by means of the  $k$ - $\epsilon$  turbulence closure model in which both the turbulent energy  $k$  and the dissipation  $\epsilon$  are computed (Rodi, 1980). The resulting vertical eddy viscosity  $\nu_T$  is variable both in time and space. For details on the  $k$ - $\epsilon$  turbulence model formulations, see Burchard *et al.* (2008).

At the bed ( $\sigma = -1$ ), a quadratic friction law is applied and the vertical velocity  $\omega$  is set to zero

$$\tau_b \equiv \rho_w \frac{v}{(H + \zeta)} \frac{\partial u}{\partial \sigma} = \rho_w u_* |u_*|, \quad \omega = 0, \quad (1.3)$$

in which  $\tau_b$  is the bed shear stress and  $u_*$  is the shear velocity that relates the velocity gradient at the bed to the velocity  $u$  in the lowest computational grid point by assuming a logarithmic velocity profile.

At the free surface ( $\sigma = 0$ ), a no-stress condition is applied and the vertical velocity  $\omega$  is set to zero

$$\rho_w \frac{v}{(H + \zeta)} \frac{\partial u}{\partial \sigma} = 0, \quad \omega = 0. \quad (1.4)$$

### 1.3.2 Sediment transport and bed evolution

The bedload transport,  $S_b$  is calculated by

$$S_b = 0.006 \alpha_s \rho_s w_s d M^{0.5} M_e^{0.7}, \quad (1.5)$$

where  $\alpha_s$  is the correction parameter for the slope effects (see below),  $\rho_s$  the specific density of the sediment,  $w_s$  the settling velocity of the sediment, and  $d$  the sediment grain size.  $M$  and  $M_e$ , respectively the sediment mobility number and excess sediment mobility number, are given by

$$M = \frac{u_r^2}{(\rho_s/\rho_w - 1)gd}, \quad M_e = \frac{(u_r - u_{cr})^2}{(\rho_s/\rho_w - 1)gd}, \quad (1.6)$$

where  $u_r$  is the magnitude of the equivalent depth-averaged velocity computed from the velocity in the bottom computational layer assuming a logarithmic velocity profile,  $u_{cr}$  is the critical depth-averaged velocity for the initiation of motion of sediment based on the Shields curve. If  $u_r < u_{cr}$ , the bed load transport is set to zero.

Bed load transport is affected by bed level gradients, which causes sediment to move more difficult upslope than downslope. The correction parameter  $\alpha_s$  for the slope effect is usually taken inversely proportional to the tangent of the angle of repose of sand  $\varphi_s$  (Sekine and Parker, 1992)

$$\alpha_s = \frac{1}{\tan \varphi_s}. \quad (1.7)$$

The angle of repose of sand  $\varphi_s$  is in the range between 15° and 30°.

The suspended load transport  $S_s$  is calculated by

$$S_s = \int_a^{(H+\zeta)} \left( uc - \varepsilon_{s,z} \frac{\partial c}{\partial x} \right) dz, \quad (1.8)$$

where  $a$  is the reference height (see below) and  $c$  is the mass concentration, defined by

$$\frac{\partial c}{\partial t} + \frac{\partial(cu)}{\partial x} + \frac{\partial(w - w_s)c}{\partial z} = \frac{\partial}{\partial x} \left( \varepsilon_{s,x} \frac{\partial c}{\partial x} \right) + \frac{\partial}{\partial z} \left( \varepsilon_{s,z} \frac{\partial c}{\partial z} \right), \quad (1.9)$$

where  $\varepsilon_{s,x}$  and  $\varepsilon_{s,z}$  are the sediment diffusivity coefficients in  $x$  and  $z$  direction, respectively. Sediment transported below the reference height  $a = 0.01H$  is regarded as bed load transport as it responds almost instantaneously to changing flow conditions (*Van Rijn, 2007*). Transport above this height is considered to be in suspension.

Finally, the bed evolution is governed by the sediment continuity equation (Exner equation), which reads

$$(1 - \varepsilon_p) \frac{\partial z_b}{\partial t} + \frac{\partial(S_b + S_s)}{\partial x} = 0, \quad (1.10)$$

in which  $\varepsilon_p = 0.4$  is the bed porosity,  $S_b$  the bed load transport (eq. (1.5)), and  $S_s$  the suspended load transport (eq. (1.8)). Equation (1.10) simply states that convergence (or divergence) of the total transport rate must be accompanied by a rise (or fall) of the bed profile.

Morphological changes occur on a much larger time-scale than the hydrodynamic changes. Therefore a morphological acceleration factor (MORFAC) is introduced. This allows for faster computations by multiplying the bed evolution after each time step by the factor (*Lesser et al., 2004*). A MORFAC of 2000 means that the bed evolution is multiplied by a factor 2000. If the model calculates one tidal period (considering a tidal period in the order of 12 hours), the morphological evolution is then simulated over 2.7 years. A sensitivity analysis is used to determine the appropriate/maximum MORFAC, given that the model results are still independent of the MORFAC (*Ranasinghe et al., 2011*). The maximum MORFAC is lowered if more non-linear forcings such as storms, wind waves and longer tidal periods are introduced.

The bottom roughness is described by the Chézy coefficient. Assuming hydraulically rough conditions, the White-Colebrook equation is used

$$C = 18 \log(12H/k_s), \quad (1.11)$$

in which  $H$  is the water depth and  $k_s$  the roughness height. Following *Cherlet et al. (2007)*, the roughness height can be evaluated by

$$k_s = 202dR_p^{-0.369}, \quad (1.12)$$

in which the Reynolds number  $R_p$  is evaluated by

$$R_p = \frac{\sqrt{(\rho_s/\rho_w - 1)gd^3}}{\nu}, \quad (1.13)$$

with  $\nu$  the kinematic viscosity of water.

### 1.3.3 Model set-up

The calculation grid has a variable resolution in both the  $x$  and  $z$  direction, see fig. 1.2. The horizontal grid size is 2 m in the centre of the domain. Towards the lateral boundaries this increases up to 1500 m, resulting in a model domain of around 50 km (fig. 1.2b). The vertical resolution is set to 60 layers. These layers have an increasing resolution towards the bed (fig. 1.2c). A sensitivity analysis showed that the model output is very sensitive to the used grid. The current settings are a result of this analysis, higher resolutions only have a minor effect on the results.

The centre of the domain comprises sinusoidal sand waves with a wave amplitude of 1% of the mean water depth (0.25 m) as initial topography. This field is multiplied by an envelope function to ensure a gradual transition from the flat bed towards the sand wave field. The initial wavelength is set to the fastest growing mode. This mode follows from short term calculations over a single tidal cycle, following *Borsje et al.* (2013). For long term calculations including residual currents, the fine grid is extended into the direction of the migration. This ensures calculations with the same accuracy over the modelling period.

Riemann boundary conditions are imposed at the lateral boundaries to prevent reflection back into the domain. The long term calculations are run with a hydrodynamic time step of 12 seconds. A MORFAC of 2000 is used, which shows similar results to lower values for the MORFAC. A tidal amplitude of  $U_{S2} = 0.65$  m/s is set with a tidal frequency of  $\sigma_{S2} = 1.45 \cdot 10^{-4}$  rad s<sup>-1</sup>. The bed slope correction parameter  $\alpha_{bs}$  is set to 3, which corresponds to an angle of repose of sand of 19°. A Chézy roughness of  $75$  m<sup>1/2</sup>/s<sup>2</sup> follows from these settings (eq. (1.11)). The changing water depth due to sand wave growth only has a small influence on the Chézy roughness, therefore this value is kept constant in space and time. The chosen settings represent typical North Sea conditions.

For the analysis of the results the migration rate is defined as the average disposition of the crest over the years. The wave height is the average distance between a crest point and the two adjacent trough points, where the trough point is defined as the centre point between the upward and leeward slope towards the crest, respectively. The wave length is the distance between two subsequent trough points, and the time scale to equilibrium is defined as the time required to evolve from 10% to 90% of the equilibrium wave height (following *Németh et al.* (2004)).

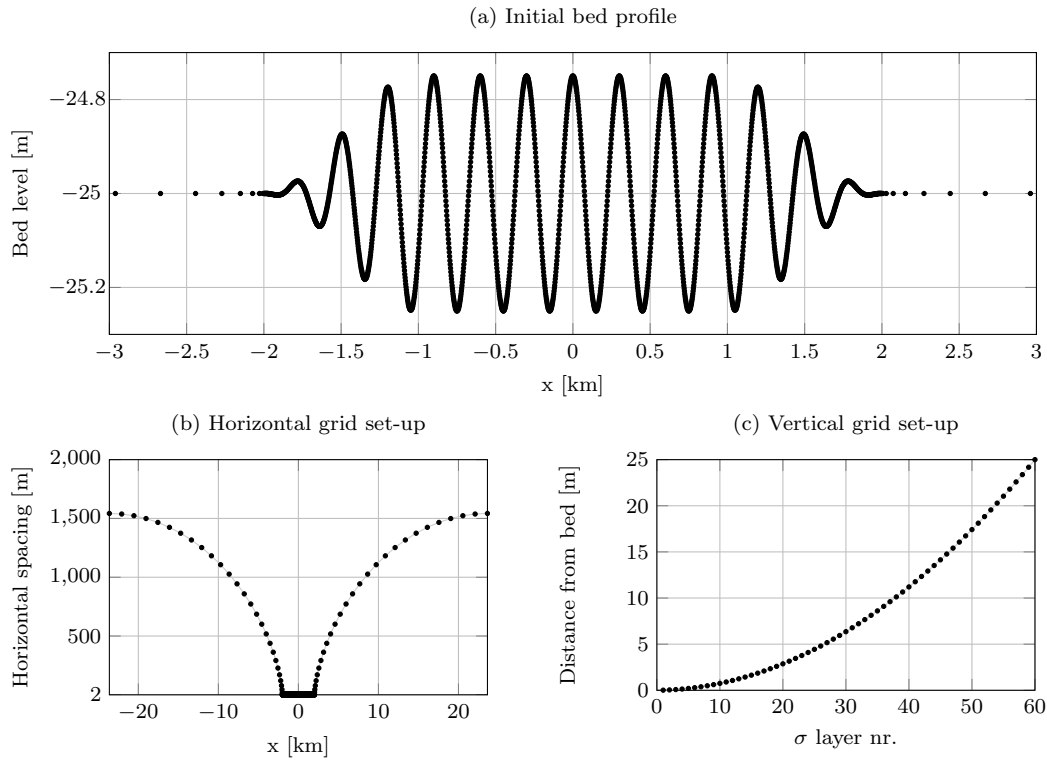


Figure 1.2 The used grid, with (a) an initial bed for a wavelength of 300 m, (b) the horizontal grid distribution for model runs with a symmetrical tide, using a fine grid in the centre where the sand waves are calculated and a coarser grid towards the boundaries and (c) the distribution of the  $\sigma$  layers over the water column, showing the distance from the bottom per layer for a mean water depth of 25 m (e.g. at  $x = -3$  km in panel (a)).

## 1.4 Results

The effects of suspended load transport and tidal asymmetry on sand wave characteristics are presented in this section. The model was run for four different combinations of model settings, as presented in table 1.1. For these field conditions, observed sand waves are typically up to 10 meters (e.g. *Besio et al.*, 2004; *Cherlet et al.*, 2007).

Table 1.1 Overview of values and dimensions of the model parameters and set-up for different tidal conditions

Description	Symbol	Value(s)	Dimension			
Tidal frequency of $S_2$ -tide	$\sigma_{S2}$	$1.45 \cdot 10^{-4}$	$\text{rad s}^{-1}$			
Chézy roughness	$C$	75	$\text{m}^{1/2}\text{s}^{-1}$			
Bed slope correction parameter	$\alpha_{bs}$	3	-			
Sediment grain size	$d$	0.35	mm			
Mean water depth	$H_0$	25	m			
Initial wave amplitude	$A_0$	0.25	m			
Timestep	$dt$	12	s			
Morphological acceleration factor	$MF$	2000	-			
<i>Model conditions:</i>		Case I	Case II	Case III	Case IV	
Amplitude of horizontal $S_0$ tidal velocity	$U_{S0}$	0	0	0.05	0.05	$\text{ms}^{-1}$
Amplitude of horizontal $S_2$ tidal velocity	$U_{S2}$	0.65	0.65	0.65	0.65	$\text{ms}^{-1}$
Fastest growing mode	$L_{FGM}$	216	204	230	216	m
Suspended load accounted for	-	No	Yes	No	Yes	-

### 1.4.1 Suspended load transport and tidal asymmetry

We start with a reference model set-up (Case I) using a symmetric tide, where only bed load sediment transport is considered. The resulting growth curve is presented in fig. 1.3. Towards the end of the simulation, the wave height is still increasing slightly, with about 5 cm per 30 years. After 150 morphological years the wave height is 9.6 m, the time scale for this height is 77 years and the sand waves show no migration.

Case II includes suspended sediment transport, which results in a slightly smaller  $L_{FGM}$  of 204 m. Equilibrium is found at a wave height of 8.6 m in a time scale of 49 years and the sand waves show no migration. This equilibrium is stable after 100 years without fluctuations in wave height when modelling the sand wave for a further hundred years.

Next, Case III considers a case with only bed load transport, including a residual current on top of the tidal forcing. Similar to Case I, the wave height is not stable at the end of the calculation. After 150 morphological years the wave height is 8.7 m, the time-scale for this height is 77 years and the migration rate is 3.2 m/year. The residual current causes both sand wave asymmetry and migration. Figure 1.3 shows that both a residual current and suspended load transport result in a reduction of the final sand wave height. Coincidentally, the reductions in wave height of Case II and III, with respect to Case I, are almost equal.

Case IV considers suspended load transport and a residual current in the tidal forcing. Here, equilibrium is reached at a wave height of 7.6 m in a time scale of 58 years and with a migration rate of 5.4 m/year. The migration rate is significantly larger with the inclusion of suspended load transport, still both the migration rate and the equilibrium wave height are in the range as observed in the field.

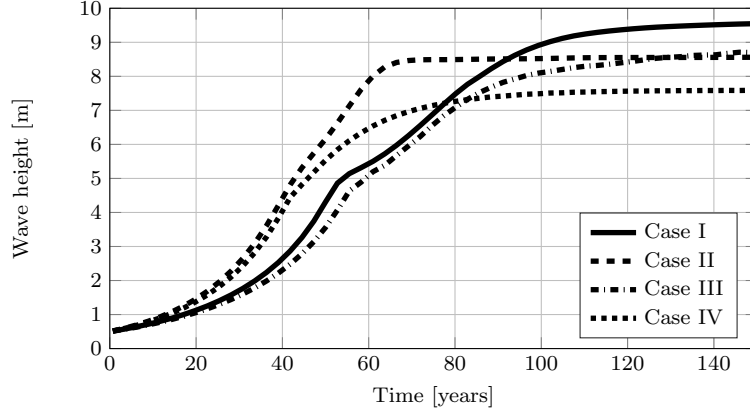


Figure 1.3 Growth curve showing the wave height development in time for different combinations of model settings, where Case II and Case IV include suspended sediment transport on top of bed load transport. Case III and Case IV include an asymmetrical tide as opposed to the symmetrical tide in Case I and Case II.

The bed evolution of Case II and Case IV is visualized in fig. 1.4, where the residual current in Case IV is imposed on the left boundary, flowing to the right. In this case, the sand waves become asymmetrical with smaller slopes on the stoss side than the lee side of the residual current direction. Additionally, the imposed  $L_{FGM}$  remains constant over the modelling period. The asterisk and dot represent the tracking of a single crest and trough over time, respectively. In fig. 1.4b the migration of the sand wave is clearly visible, the crest has moved 520 m in the direction of the residual current after 100 morphological years. The asymmetry of the bed for Case IV is comparable with seabed profiles as found by *Besio et al.* (2004), although the crests here are slightly more rounded.

### 1.4.2 Residual current strength

Next, the influence of the residual current strength on the wave height for Case II is studied. An increasing residual current strength results in a larger  $L_{FGM}$  due to the increasing importance of suspended sediment and larger flow velocities, for example the  $L_{FGM}$  is 204 m for the symmetrical case (Case II) and 326 m with a residual current strength of 0.2 m/s. The effect on the equilibrium sand wave height is shown in fig. 1.5, a decrease in wave height is predicted for larger values of the residual current. For smaller residual currents this effect is small, and for larger residual currents the effect also decreases. For North Sea conditions the residual current

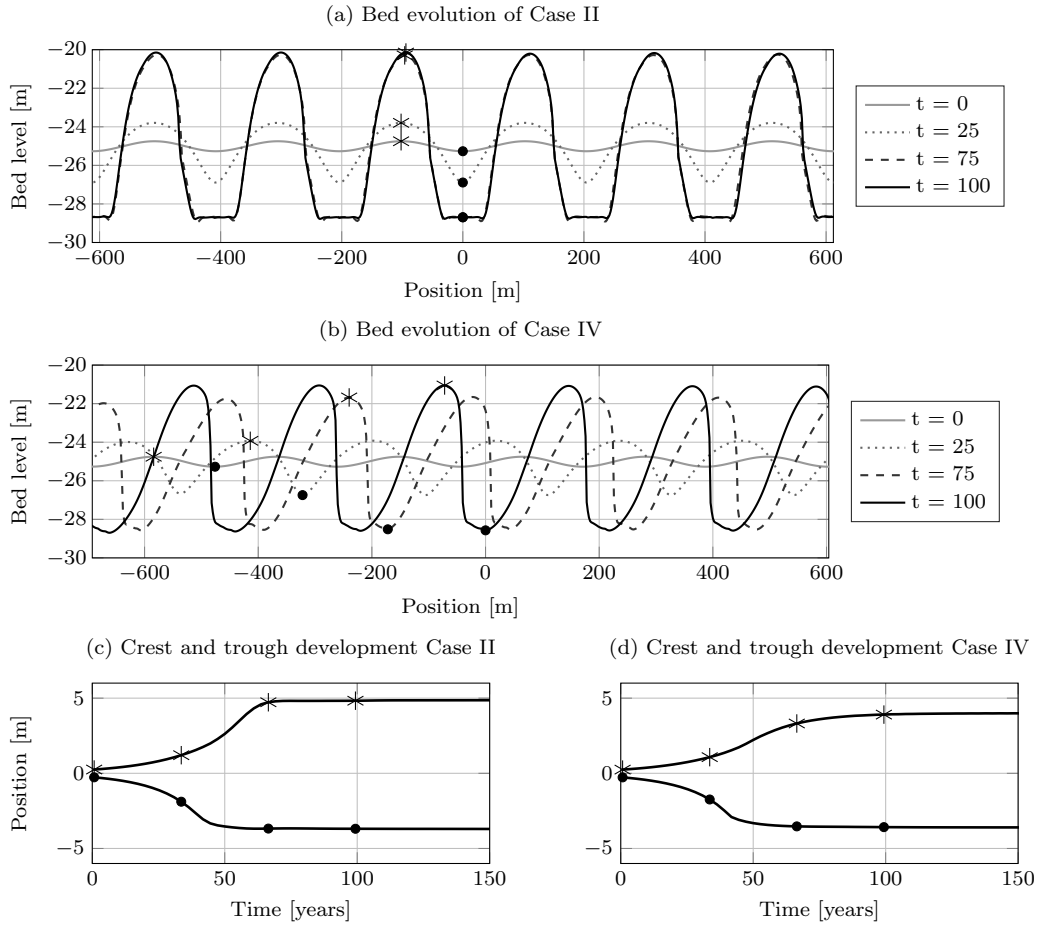


Figure 1.4 Bed evolution in time, of (a) a symmetrical (Case II) and (b) an asymmetrical case (Case IV) both including suspended load transport. The relative growth to the initial water depth of the crest and trough points is depicted for (c) Case II and (d) Case IV. In all figures the location of the crest and trough points is tracked with an asterisk and dot, respectively.

strength will not exceed 0.2 m/s, *Buijsman and Ridderinkhof (2007)* found values of up to 0.15 m/s in the field. The used conditions show a linear increase of the migration rate with an increasing  $U_{S0}$ . Before equilibrium is reached, the migration rate is not constant in time because the sand waves are still changing in asymmetry. After equilibrium is reached, the migration rate is constant in time.

Using a residual current on top of a constant symmetrical tide increases and decreases the maximum and minimum- tidal excursion, respectively. This does affect the outcomes, but cannot be compared to an increase in flow velocities, as also found by *Sterlini et al. (2009)*. This was tested by reducing the amplitude of the symmetrical tide such that the maximum flow velocity for the asymmetrical

case equalled the original symmetrical tide ( $U_{S0} = 0.05$  m/s,  $U_{S2} = 0.60$  m/s). This caused a further reduction in wave height. Decreasing the flow velocity for a symmetrical case also decreases the wave height, but to a lesser extent (not plotted here).

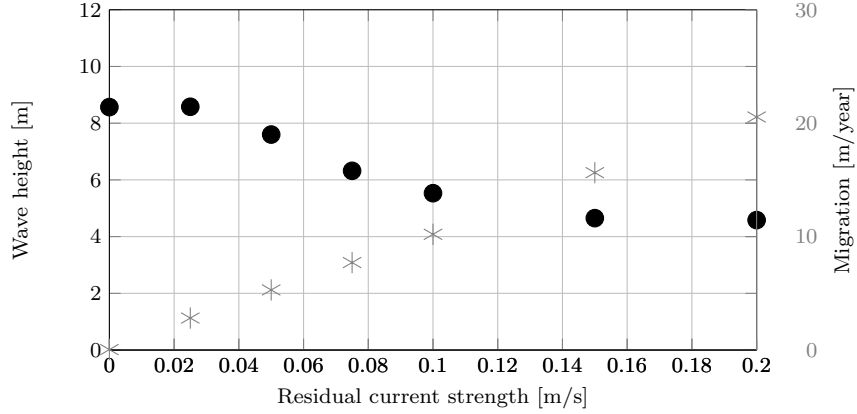


Figure 1.5 Influence of the residual current strength on the (left, dots) equilibrium wave height and (right, asterisks) migration rate.

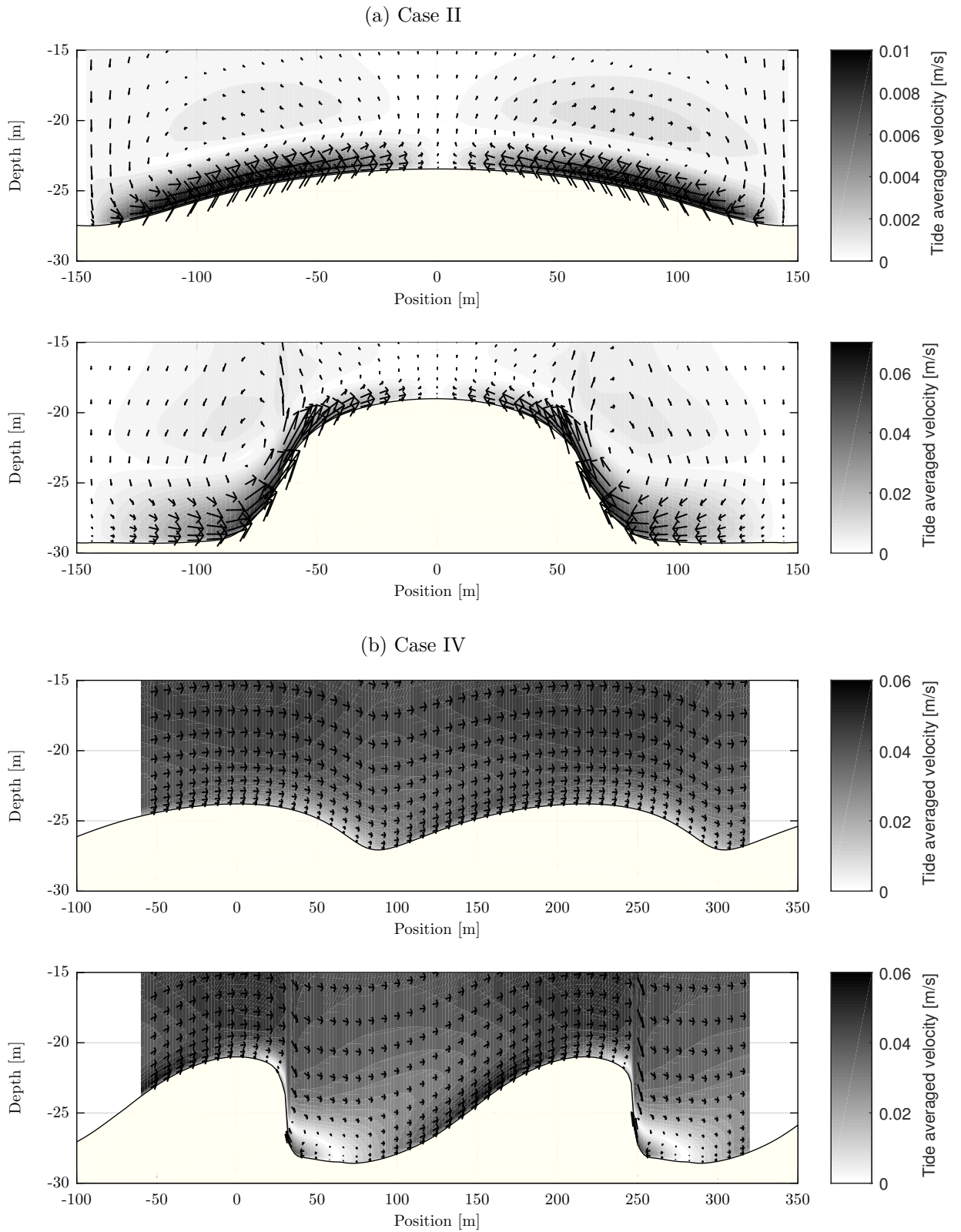
### 1.4.3 Physical explanation

As shown by *Hulscher (1996)*, sand wave growth can be explained by the presence of circulation cells. For a symmetrical tide this circulation cell results in a net convergence of sediment towards the crest, counteracted by the slope effect. In fig. 1.6a the tide averaged flow velocity amplitude is plotted. The circulation cells are clearly visible for the symmetrical case with suspended sediment (Case II). The upper figure shows the circulation cells during the growth of the bed form, while the lower figure shows the circulation cells for the equilibrium bed. Although the velocities are larger for this case, the steeper slopes have caused a balance in the driving and opposing forces.

The inclusion of suspended sediment transport has a dampening effect on the growth of sand waves, as shown by *Borsje et al. (2014)*. For the here used model settings, the inclusion of suspended sediment transport (Case II) hardly leads to a difference in the  $L_{FGM}$ . However, suspended sediment transport has a significant impact on the equilibrium sand wave height. By including suspended sediment transport, the total transport rate increases. For the grain size used in this model simulation ( $d = 0.35$  mm), the suspended sediment is transported close to the bed and thereby behaves as bed load transport, resulting in higher initial growth rates, compared to the default simulation (Case I) (see fig. 1.3). However, as soon as sand waves grow in amplitude, the suspended transport rate increases in magnitude and is at the same time transported through a larger portion of the water column. Leading to a dampening effect of the suspended sediment and resulting in lower wave heights

compared to the default model settings (Case I).

An explanation for the lower wave heights due to tidal asymmetry can be found in the hydrodynamics. A residual current causes a disturbance of the circulation cells such that convergence of sediment no longer occurs on the crest. A tide averaged flow in the direction of the residual current over the crest is observed. During the flood phase the velocities on the lee side of the sand wave are slightly lower than on the stoss side due to an increasing and decreasing water depth, respectively. During the ebb phase the opposite is observed, however, the tidal amplitude of the ebb phase is lower. Tide averaged flow velocities on the stoss side are therefore larger than on the lee side. This residual flow causes a net transport in the direction of the residual current, which translates into migration and asymmetry of the bed form. Because this average flow is not uniform over the bed, convergence of sediment occurs at the points of smaller flow velocities, after the crest. This is shown in fig. 1.6b, where the lower figure is the equilibrium bed again and the upper figure the bed during growth. The contour plot shows that on the lee side and on the crest of the sand wave the flow velocities are smaller. This is more distinguished in the equilibrium (lower) plot as the slopes are steeper here. Furthermore, the threshold of motion for sediment transport is exceeded for a longer period of time during the flood phase. This all makes that sediment transport towards the sand wave crest is mostly coming from one side instead of two sides, as we saw in the symmetrical case.



15

Figure 1.6 Tide averaged flow velocity amplitudes over sand waves during (upper) growth and (lower) equilibrium for (a) a symmetrical case (Case II) and (b) an asymmetrical case (Case IV) including suspended load.

## 1.5 Discussion

The here used numerical shallow water model Delft3D has already shown that the initial stages of sand wave growth can be predicted. This is the first model study that studied the growth of a sand wave field towards a stable equilibrium. The influence of physical processes on the growth and equilibrium height of sand wave fields has been studied. It was found that both suspended load transport and tidal asymmetry are essential processes that cannot be neglected in equilibrium sand wave modelling. *Sterlini et al. (2009)* also found that tidal asymmetry has a dampening effect on the sand wave height.

The model predictions are very sensitive to the model- and process parameters. Various parameters are found to have an influence in the order of meters on the equilibrium wave height (e.g. the nr. of  $z$  layers, horizontal spacing  $dx$ , Chézy roughness  $C$ , slope parameter  $\alpha_{bs}$ , tidal amplitude  $U_{S2}$ , mean water depth  $H_0$  and grain size  $d$ , not plotted here). The initial bed also influences the outcomes. This is because most growth curves (for determining the  $L_{FGM}$ ) showed a small difference in maximum growth rate for a range of wave lengths. Because of this small difference, these wave lengths prevailed in the long term when they were imposed as initial bed for equilibrium calculations. Smaller values of the  $L_{FGM}$  resulted in smaller wave heights than larger values of the  $L_{FGM}$ , all these model runs reached a stable equilibrium.

Another process that may have an effect on the model outcomes is the chosen transport formula, which describes the initiation of motion. The initiation of motion of sediment particles is very important for the balance between the driving and restoring forces, small changes in the definition of this process may affect the growth and equilibrium of sand waves. Furthermore, the definition of suspended load, using a reference height  $a = 0.01H$ , also has an effect on the transport and could therefore influence the results. These processes are model constants so their influence on the results was not verified.

To reduce the influence of the grid on the model outcomes, a grid refinement study has been conducted. Compared to *Borsje et al. (2013, 2014)* this resulted in a finer grid with more  $z$  layers and a smaller  $dx$ . Although the new grid lead to different results for the short time scale, the physical processes as described in the papers of *Borsje et al. (2013, 2014)* are unchanged. A more refined grid was mainly required for longer time scales. To reduce calculation times we therefore used a coarser grid in  $x$ -direction for shorter time scales (for determining the  $L_{FGM}$ ). With the newly defined grid, the  $L_{FGM}$  became smaller than realistic for the input parameters, this was compensated for by an increased  $\alpha_{bs}$ .

A direct result of the numerical modelling is that numerical instability may occur. Here, the grid has been optimized for a case where suspended load transport was included in the transport equations. For calculations without suspended load the troughs showed discontinuities in the form of extra erosion at the bottom of the slope. Smaller values of  $dx$  suppressed this effect due to a more gradual transition of

the flow velocities over the bed. Suspended load transport reduced the presence of these discontinuities, and therefore allowed for a coarser grid. The definition of the trough location reduced the effect of these discontinuities on the growth curve, but the effect is still apparent in fig. 1.3 (bump in growth rate at a wave height of 5 m for Cases I and III).

The introduction of a MORFAC is very convenient as it allows for long-term calculations, but it has a few limitations. As indicated by *Ramasinghe et al.* (2011), complex real-life situations may require significantly smaller MORFAC values. The introduction of a spring-neap tide is therefore not possible in the current set-up. Combining the  $S_2$  and  $M_2$  components would result in a tidal forcing that varies on a much larger time scale. To achieve a similar accuracy, the MORFAC would need to be reduced accordingly. Furthermore, the total transport rates during one spring-neap cycle for (1) a spring-neap case and (2) a simplified case with only a  $S_2$  component differ significantly. This has an effect on the formation and growth towards equilibrium of sand waves. *Blondeaux and Vittori* (2010) found a 30% difference in  $L_{FGM}$  between the two cases. As also found by *Sterlini et al.* (2009), the currently used flow conditions predict the basic dimensions of the sand waves correctly. However, inclusion of other processes may result in sand waves of different shapes and sizes.

Another process that could improve the predictive capabilities of sand wave models are wind waves and storms *Campmans et al.* (see e.g. 2016). To this end, a switch from 2DV to 3D is recommended, which allows investigating flows and wind waves that are not perpendicular to the bed form. Further processes that are excluded here that may lead to better representations of sand wave growth are grain sorting (as discussed by *Roos et al.*, 2007; *Van Oyen and Blondeaux*, 2009) and the inclusion of biota (as discussed by *Borsje et al.*, 2009). Both processes are currently being investigated in the framework of the SANDBOX programme (*Damveld et al.*, 2015). Despite the exclusion of these additional non-linear processes, the simulated sand wave growth gives a good indication of the possible growth with equilibrium wave heights in the range of field observations.

Although we are able to model sand waves from an initial perturbation to an equilibrium, it requires large computational efforts. This is a downside of the numerical shallow water model, the use of non-linear stability models (e.g. *Van den Berg et al.*, 2012) may therefore be more appropriate for the modelling of the long-term qualitative evolution of sand waves. This model would still require the inclusion of suspended load transport together with a turbulence closure model that allows for variation of the eddy viscosity both in time and space. The here presented model could then be used for detailed short-term predictions. Further research into the self organisational properties of the model by imposing a random initial bed is recommended.

## 1.6 Conclusions

A numerical shallow water model (Delft3D) has been used to describe the growth towards the equilibrium of sand waves in a sand wave field. The model was able to calculate a stable equilibrium from an initial disturbance on a large domain. For this a careful treatment of the grid was required, together with the inclusion of suspended load sediment transport.

The model results showed that suspended load transport and tidal asymmetry each had a significant dampening effect on the equilibrium wave height. When these processes were combined, the wave height was reduced even further. The growth of sand waves can be explained by the formation of tide averaged circulations cells. Tidal asymmetry disturbs this mechanism such that convergence of sediment no longer occurs on top of the crest, but downstream of this point, which causes migration and asymmetry of the bed forms.

# Bibliography

- Besio, G., P. Blondeaux, and P. Frisina (2003), A note on tidally generated sand waves, *Journal of Fluid Mechanics*, 485, 171–190, doi:10.1017/S0022112003004415.
- Besio, G., P. Blondeaux, M. Brocchini, and G. Vittori (2004), On the modeling of sand wave migration, *Journal of Geophysical Research C: Oceans*, 109(4), C04,018, doi:10.1029/2002JC001622.
- Besio, G., P. Blondeaux, and G. Vittori (2006), On the formation of sand waves and sand banks, *Journal of Fluid Mechanics*, 557, 27, doi:10.1017/S0022112006009256.
- Besio, G., P. Blondeaux, M. Brocchini, S. J. M. H. Hulscher, D. Idier, M. A. F. Knaapen, A. A. Németh, P. C. Roos, and G. Vittori (2008), The morphodynamics of tidal sand waves: A model overview, *Coastal Engineering*, 55(7-8), 657–670, doi:10.1016/j.coastaleng.2007.11.004.
- Blondeaux, P., and G. Vittori (2005a), Flow and sediment transport induced by tide propagation: 1. The flat bottom case, *Journal of Geophysical Research C: Oceans*, 110(7), 1–13, doi:10.1029/2004JC002532.
- Blondeaux, P., and G. Vittori (2005b), Flow and sediment transport induced by tide propagation: 2. The wavy bottom case, *Journal of Geophysical Research C: Oceans*, 110(8), 1–11, doi:10.1029/2004JC002545.
- Blondeaux, P., and G. Vittori (2010), Formation of tidal sand waves: Effects of the spring-neap cycle, *Journal of Geophysical Research: Oceans*, 115(10), doi:10.1029/2010JC006400.
- Borsje, B. W., M. B. De Vries, T. J. Bouma, G. Besio, S. J. M. H. Hulscher, and P. M. J. Herman (2009), Modeling bio-geomorphological influences for offshore sandwaves, *Continental Shelf Research*, 29(9), 1289–1301, doi:10.1016/j.csr.2009.02.008.
- Borsje, B. W., P. C. Roos, W. M. Kranenburg, and S. J. M. H. Hulscher (2013), Modeling tidal sand wave formation in a numerical shallow water model: The role of turbulence formulation, *Continental Shelf Research*, 60, 17–27, doi:10.1016/j.csr.2013.04.023.

- Borsje, B. W., W. M. Kranenburg, P. C. Roos, and S. J. M. H. Hulscher (2014), The role of suspended load transport in the occurrence of tidal sand waves, *Journal of Geophysical Research : Earth Surface*, *119*(4), 701–716, doi:10.1002/2013JF002828.
- Buijsman, M. C., and H. Ridderinkhof (2007), Long-term ferry-ADCP observations of tidal currents in the Marsdiep inlet, *Journal of Sea Research*, *57*(4), 237–256, doi:10.1016/j.seares.2006.11.004.
- Burchard, H., P. D. Craig, J. R. Gemmrich, H. van Haren, P. P. Mathieu, H. E. M. Meier, W. A. M. N. Smith, H. Prandke, T. P. Rippeth, E. D. Skyllingstad, W. D. Smyth, D. J. S. Welsh, and H. W. Wijesekera (2008), Observational and numerical modeling methods for quantifying coastal ocean turbulence and mixing, *Progress in Oceanography*, *76*(4), 399–442, doi:10.1016/j.pocean.2007.09.005.
- Campmans, G. H. P., P. C. Roos, H. J. De Vriend, and S. J. M. H. Hulscher (2016), Modeling the influence of storms on sand wave dynamics : a linear stability approach, *Submitted to Continental Shelf Research*.
- Cherlet, J., G. Besio, P. Blondeaux, V. Van Lancker, E. Verfaillie, and G. Vittori (2007), Modeling sand wave characteristics on the Belgian Continental Shelf and in the Calais-Dover Strait, *Journal of Geophysical Research*, *112*(C6), C06,002, doi:10.1029/2007JC004089.
- Damveld, J. H., B. W. Borsje, P. C. Roos, and S. J. M. H. Hulscher (2015), Smart and sustainable design for offshore operations in a sandy seabed - the SANDBOX programme, in *MARID V*, April.
- Dodd, N., P. Blondeaux, D. Calvete, H. E. De Swart, A. Falqués, S. J. M. H. Hulscher, G. Rózyński, and G. Vittori (2003), Understanding Coastal Morphodynamics Using Stability Methods, *Journal of Coastal Research*, *19*(4), 849–865.
- Dyer, K. R., and D. A. Huntley (1999), The origin, classification and modelling of sand banks and ridges, *Continental Shelf Research*, *19*(10), 1285–1330, doi:10.1016/S0278-4343(99)00028-X.
- Gerkema, T. (2000), A linear stability analysis of tidally generated sand waves, *Journal of Fluid Mechanics*, *417*(September 2013), 303–322, doi:10.1017/S0022112000001105.
- Hulscher, S. J. M. H. (1996), Tidal-induced large-scale regular bed form patterns in a three-dimensional shallow water model, doi:10.1029/96JC01662.
- Knaapen, M. A. F. (2005), Sandwave migration predictor based on shape information, *Journal of Geophysical Research: Earth Surface*, *110*(4), doi:10.1029/2004JF000195.

- Komarova, N. L., and S. J. M. H. Hulscher (2000), Linear instability mechanisms for sand wave formation, *Journal of Fluid Mechanics*, 413, 219–246, doi:10.1017/S0022112000008429.
- Lesser, G. R., J. A. Roelvink, J. A. T. M. van Kester, and G. S. Stelling (2004), Development and validation of a three-dimensional morphological model, *Coastal Engineering*, 51(8-9), 883–915, doi:10.1016/j.coastaleng.2004.07.014.
- McCave, I. N. (1971), Sand waves in the North Sea off the coast of Holland, *Marine Geology*, 10(3), 199–225, doi:10.1016/0025-3227(71)90063-6.
- Németh, A. A., S. J. M. H. Hulscher, and H. J. De Vriend (2002), Modelling sand wave migration in shallow shelf seas, *Continental Shelf Research*, 22(18-19), 2795–2806, doi:10.1016/S0278-4343(02)00127-9.
- Németh, A. A., S. J. M. H. Hulscher, and H. J. De Vriend (2003), Offshore sand wave dynamics, engineering problems and future solutions.
- Németh, A. A., S. J. M. H. Hulscher, and R. M. J. Van Damme (2004), Modelling sand wave migration and height, comparing model results and data, in *Marine Sandwave and River Dune Dynamics*, April, pp. 232–239.
- Németh, A. A., S. J. M. H. Hulscher, and R. M. J. Van Damme (2006), Simulating offshore sand waves, *Coastal Engineering*, 53(2-3), 265–275, doi:10.1016/j.coastaleng.2005.10.014.
- Németh, A. A., S. J. M. H. Hulscher, and R. M. J. Van Damme (2007), Modelling offshore sand wave evolution, *Continental Shelf Research*, 27(5), 713–728, doi:10.1016/j.csr.2006.11.010.
- Ranasinghe, R., C. Swinkels, A. Luijendijk, D. Roelvink, J. Bosboom, M. Stive, and D. Walstra (2011), Morphodynamic upscaling with the MORFAC approach: Dependencies and sensitivities, *Coastal Engineering*, 58(8), 806–811, doi:10.1016/j.coastaleng.2011.03.010.
- Rodi, W. (1980), *Turbulence models and their application in hydraulics - A state of the art review*, 115 pp., University of Karlsruhe, Karlsruhe, Germany.
- Roos, P. C., and S. J. M. H. Hulscher (2003), Large-scale seabed dynamics in offshore morphology: Modeling human intervention, *Reviews of Geophysics*, 41(2), 1010, doi:10.1029/2002RG000120.
- Roos, P. C., S. J. M. H. Hulscher, F. Van der Meer, T. A. G. P. Van Dijk, I. G. M. Wientjes, and J. H. Van den Berg (2007), Grain size sorting over offshore sandwaves : Observations and modelling, in *Fifth IAHR Symp. on River, Coastal and Estuarine Morphodynamics*, pp. 649–656, University of Twente, The Netherlands.

- Sekine, M., and G. Parker (1992), Bed-load transport on transverse slope, *Journal of Hydraulic Engineering*, 118(4), 513–535.
- Sterlini, F., S. J. M. H. Hulscher, and D. M. Hanes (2009), Simulating and understanding sand wave variation: A case study of the Golden Gate sand waves, *Journal of Geophysical Research*, 114(F2), F02,007, doi:10.1029/2008JF000999.
- Terwindt, J. H. J. (1971), Sand waves in the southern bight of the North Sea, *Marine Geology*, 10(1), 51–67, doi:10.1016/0025-3227(71)90076-4.
- Van den Berg, J. H., F. Sterlini, S. J. M. H. Hulscher, and R. M. J. Van Damme (2012), Non-linear process based modelling of offshore sand waves, *Continental Shelf Research*, 37, 26–35, doi:10.1016/j.csr.2012.01.012.
- Van Oyen, T., and P. Blondeaux (2009), Grain sorting effects on the formation of tidal sand waves, doi:10.1017/S0022112009006387.
- Van Rijn, L. C. (2007), Unified View of Sediment Transport by Currents and Waves. I: Initiation of Motion, Bed Roughness, and Bed-Load Transport, *Journal of Hydraulic Engineering*, 133(6), 649–667, doi:10.1061/(ASCE)0733-9429(2007)133:6(649).

## Appendix A

# Sensitivity of results to various parameters

The sensitivity of the bed evolution to various model parameters and process parameters are presented.

Figure A.1 shows the sensitivity of various model parameters on sand wave growth. For a grid spacing of  $dx = 1$  m the run becomes unstable, which leads to unrealistic growth on part of the domain and complete absence of further growth for the sand wave shown here. The number of  $z$ -layers (fig. A.1b) shows several things. The transport rates reduce with an increasing number of  $z$ -layers. For 20  $z$ -layers the larger transport rates have a stabilizing effect, resulting in very low and long sand waves ( $L_{FGM} = 750$  m). For 30  $z$ -layers, the transport rates are still larger than for more layers, however, low enough for sand waves to grow. The initial ratio between bed load transport and suspended load transport is larger, which leads larger sand wave heights due to a smaller influence of suspended load transport. The difference between the results of 60 and 90  $z$ -layers is minimal for the equilibrium height. The time-scale to equilibrium reduces with an increase in  $z$ -layers.

The range in wave height between a MORFAC of 500 and 3000 is less than half a meter (fig. A.1c). While the initial growth of these bottom forms show the same behaviour, the equilibrium height differs. For larger MORFAC values the wave height is reduced.

This sensitivity analysis (fig. A.1) showed that the number of  $z$ -layers still had a large influence on the equilibrium height. Therefore, all calculations presented in the main text were run with 60 layers instead of the earlier adopted 30 layers. A sensitivity analysis of various process parameters was also conducted with 60  $z$ -layers, here we used a MORFAC of 3000, see fig. A.2. The figure shows that changes in these parameters have a large effect on the equilibrium height. The effect of  $d$  and  $\alpha_{bs}$  appears smaller, but it should be kept in mind that all processes affect the  $L_{FGM}$ , which in turn also affects the height (as shown in fig. A.2f). Furthermore, the Chézy roughness is a function of the grain size and water depth, but here we kept the roughness constant. Therefore the effect of these processes may be also change.

Because the exact value of (some) of these parameters can vary both in space and time, it is difficult to compare the model results with field conditions.

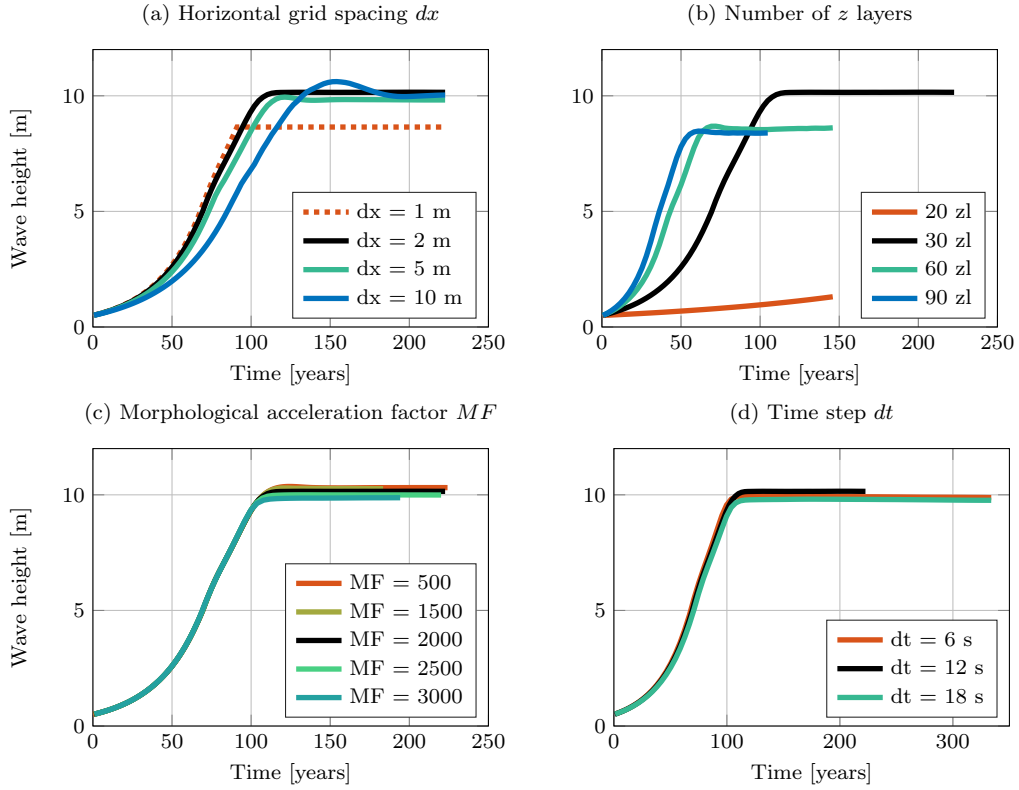


Figure A.1 Sensitivity of various model settings on the wave growth. With in (a) the influence of the grid spacing  $dx$ , (b) the number of  $z$ -layers, (c) the morphological acceleration factor  $MF$  and (d) the calculation time step  $dt$ . The used parameters in the model (Case II) are coloured black, all calculations (except (b)) used 30 $z$ -layers.

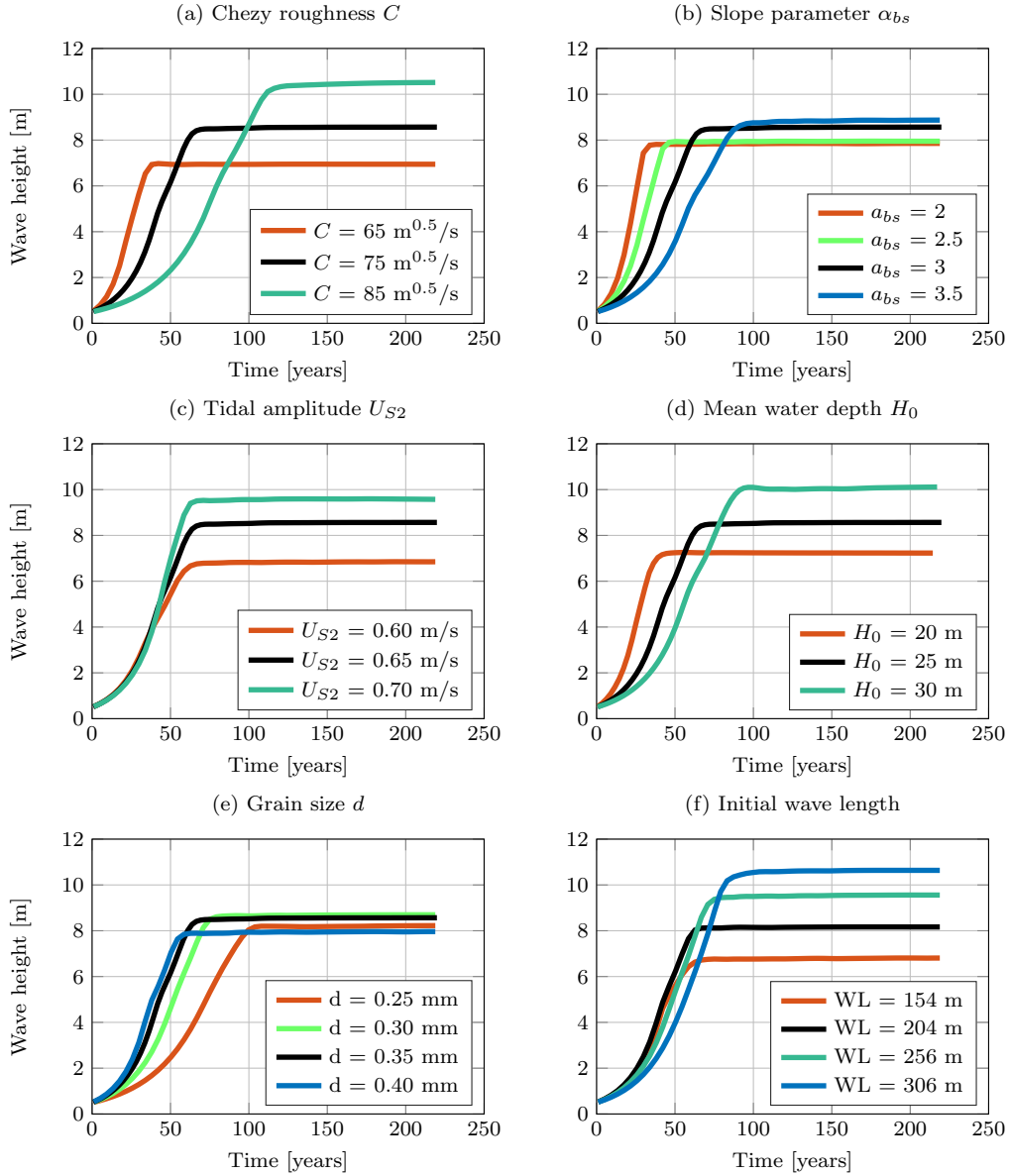


Figure A.2 Sensitivity of various process parameters on the wave growth. With in (a) the influence of the Chézy roughness  $C$ , (b) the slope parameter  $\alpha_{bs}$ , (c) the tidal amplitude  $U_{S2}$ , (d) mean water depth  $H_0$ , (e) grain size  $d$  and (f) the initial wave length. The used parameters in the model (Case II) are coloured black.

## Appendix B

# Data analysis of field measurements after a dredging event

For two dredging locations in the Belgian continental shelf the bathymetry has been monitored before and after dredging. This could provide insight in growth rates of sand waves in the field, which is useful for the calibration of equilibrium sand wave models. The method for analysing this data is described below, after which the results are presented. We would like to acknowledge Koen Degrendele of the Federal Public Service of Belgium and Vera van Lancker of the Royal Belgian Institute of Natural Sciences for making the data available.

### B.1 Method

The data has a variable resolution of around 1  $m$ , and is available as  $XYZ$  point data. With the use of Delaunay triangulation, the bed profiles are plotted. To better monitor the growth in time, several transects are selected in line with the dredged area. A selection based on the direction of the sand wave propagation is not feasible due to the size and shape the measured areas and the large variability of sand wave direction therein. The current selection method may result in larger sand wave lengths, but the transects are mostly in line with the bed perturbations. Because the interest of this study is mostly to the growth speed this does not impact the results.

Next, the measured depth values along the transect are extracted, resulting in a bottom profile. This profile is linearly interpolated to obtain evenly spaced points.

On these profiles a Fourier analysis is performed, which shows the distribution of the frequency spectrum. The smaller and larger bed forms are then filtered out, in this way only the sand waves are analysed. This is done via Butterworth filtering. Both a low- and high-pass filter are used, filtering bed forms outside the range of wave lengths between 50  $m$  and 1200  $m$ .

The wave characteristics are determined by semi-automatic selection of trough and crest points from the transects. Trough and crest point are selected between points where the signal crosses its mean with a positive slope. It is possible that this method also selects local maxima and minima that are not real crest and trough points. If this occurs, these points are removed manually. With these crest and trough points the wave height and length is calculated, with which a growth curve is plotted in time.

## B.2 Results

Of the two monitored areas, both a transect in the dredged area as well as the area between the dredged part and the deeper section have been analysed (fig. B.1). The applied filtering to these transects was based on a 4<sup>th</sup> order Butterworth filter, with cut-off frequencies at 1/50 and 1/1500 for the low- and high-pass filter respectively. The result of this filtering on the bed profile is shown in fig. B.2 for one of the transects.

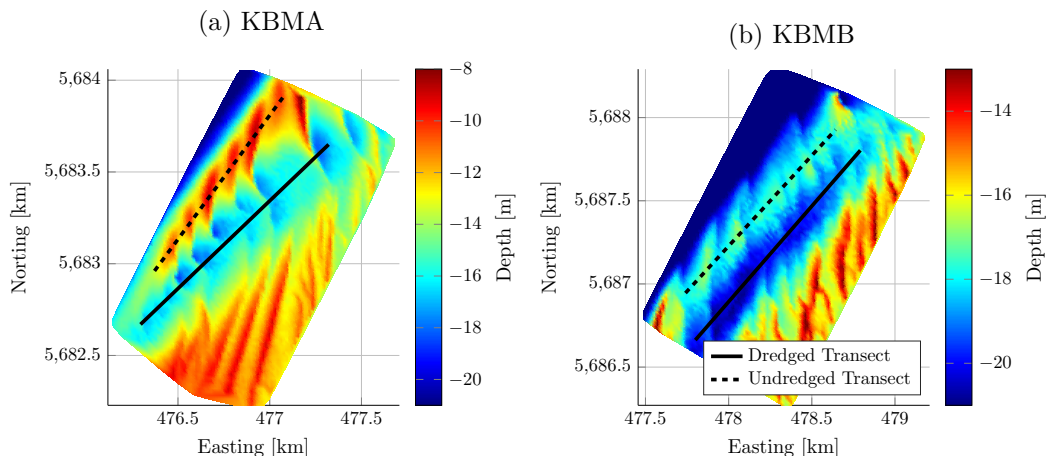


Figure B.1 Bed profiles and used transects of field measurements in the Belgium Continental Shelf. Here shown profiles were measured in 2012.

For every transect the bed evolution in time is analysed and from this only sand waves are selected that are present during the whole time of measuring. Sand waves that migrated in and out of the domain during measurements were therefore not considered. Furthermore, the dredged channel of location KBMA showed formation of sand waves in the later measurements. Growth of these waves is therefore only recorded for later transects. Figure B.3 shows the bed evolution and wave growth of this transect.

The sand waves in non-dredged parts of the terrain are assumed to be in equilibrium. Therefore the sand wave height is also tracked for these locations. For location KBMA this is shown in fig. B.4. In the dredged transect (fig. B.3) two waves show an average growth rate of  $0.28 \text{ m/yr}$ , with wave heights of up to three meter it would

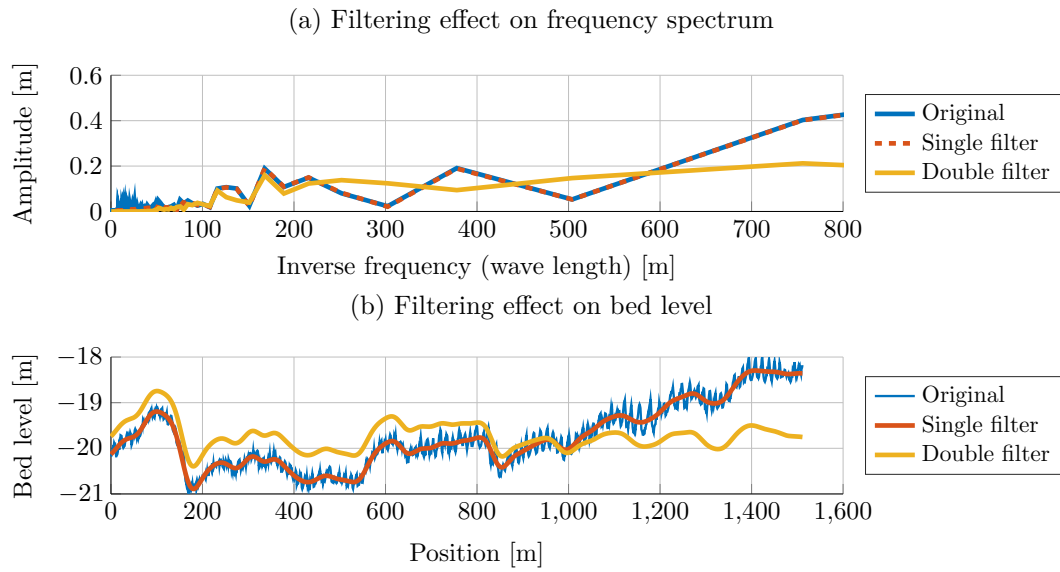


Figure B.2 Filtering of the dredged KBMB transect of year 2012. Single filter is only low-pass, where the double filter also filtered out the lower frequencies (higher wavelengths).

require only a few extra years to reach sand waves of the maximum found amplitude of up to 4.5  $m$ , as found in the undredged transect. Using the growth rate of 0.28  $m$  per year, it would require 16 years to reach equilibrium height, starting from a flat bed.

The wave height of the undredged transect shows large variation in time, with variations of up to 1  $m$  per year. This shows that sand waves are indeed dynamic bed forms. A possible cause for this can lie in the changed hydrodynamics, because the undredged transect lies between two deeper parts.

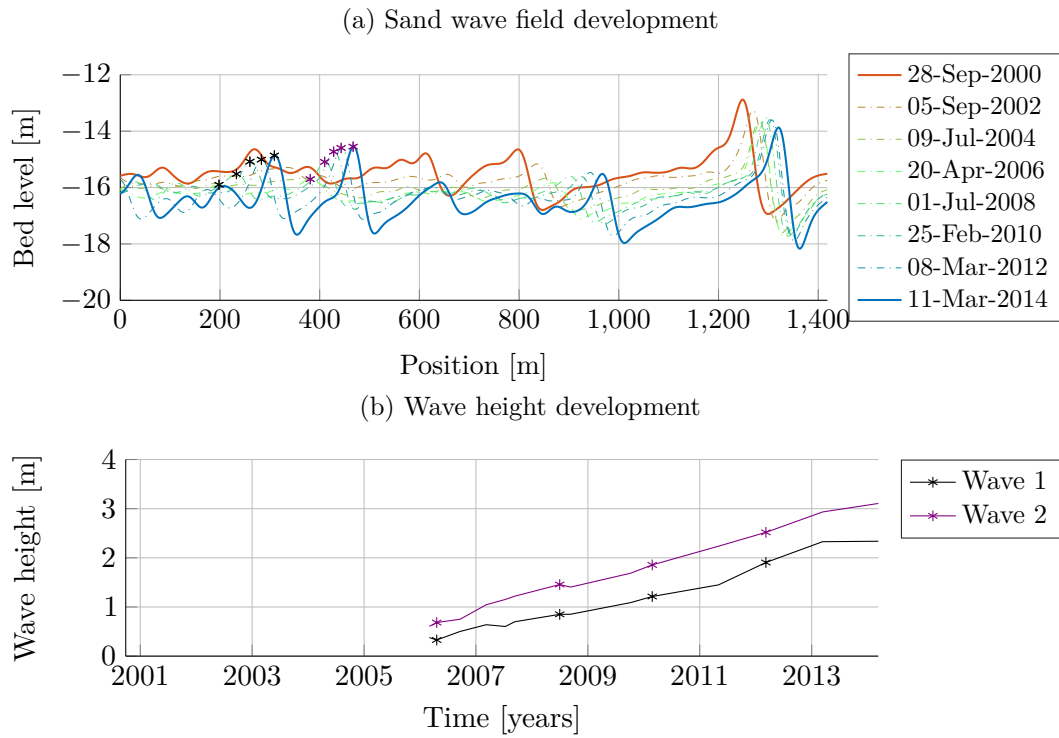


Figure B.3 Sand wave field development with indication of tracked crest points (upper) the corresponding wave height development is shown in the lower figure. Asterisks indicate the crest point at a time step in both figures.

### B.3 Conclusion

Based on the results, the growth rate of dredged sand waves is in the order of  $0.3 \text{ m/yr}$ . With these growth rates, sand waves reach their equilibrium wave height from a flat bed in only a few decades.

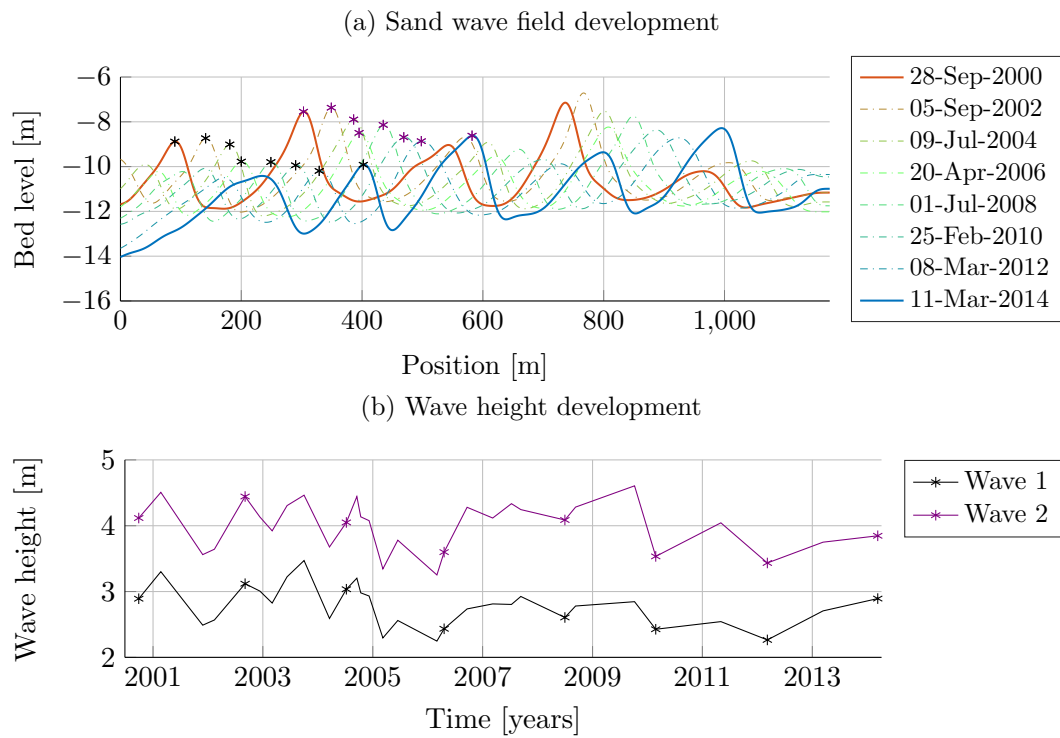


Figure B.4 Sand wave field development with indication of tracked crest points (upper) the corresponding wave height development is shown in the lower figure. The plotted tracked crest points in the upper figure are also plotted in the lower figure.